Photochemical & Photobiological Sciences

RSC Publishing

PAPER

Laser flash photolysis study of photocatalytic properties of pillared interlayered clays and Fe,Al-silica mesoporous catalysts

Cite this: *Photochem. Photobiol. Sci.*, 2013, **12**, 1939

Evgeni M. Glebov,*[a,b] Ivan P. Pozdnyakov,[a,b] Vjacheslav P. Grivin,[a] Victor F. Plyusnin,[a,b] Nikolai M. Bazhin,[a] Xu Zhang,[c] Feng Wu[c] and Maria N. Timofeeva[d,e]

Received 12th April 2013,
Accepted 2nd July 2013

DOI: 10.1039/c3pp50112d

www.rsc.org/pps

Laser flash photolysis was applied to determine the primary photochemical processes over iron-containing clay (montmorillonite KSF), pillared interlayered clays (PILCs) and mesoporous mesophase iron silicate materials (MMMs). For KSF, the homogeneous photochemical reaction of Fe(III) leached from the clay material resulted in the formation of OH radicals, which were monitored by means of their reaction with methyl viologen dication (MV^{2+}). For PILCs and MMMs, no leaching of Fe(III) to the solution nor hydroxyl radical formation were observed. Nevertheless, these catalysts were found to exhibit a sufficient effect on phenol photoionization. The increase in quantum yields of PhO radicals is caused by the effect of PILCs and MMMs and is explained by heterogeneous processes on the surface of catalyst particles.

1. Introduction

It is well-known that clays and clay materials are widely used as adsorbents and catalysts for a large diversity of industrial processes, including the pharmaceutical industry, cosmetics, organic synthesis and environmental remediation.[1,2] The treatment and purification of industrial wastewater containing toxic organic pollutants are the main fields for the catalytic clay mineral applications.[3,4] Clay-induced photochemistry plays an important role in the self-purification of natural aqueous systems. Both Fenton-like and direct photooxidation of organic impurities assisted by iron-rich clays are possible. There are several reports on the photodegradation and photooxidation of organic compounds using natural clay[5–8] or clay modified by different reagents such as dyes[9] and/or metals[9,10] and cationic surfactants[11] to enhance both the adsorption of organic pollutants and the generation of singlet oxygen.

There are only a few reports in the literature concerning the mechanistic investigation of clay photocatalysis. Xiong *et al.*[9,11] reported the formation of singlet oxygen in the course of photocatalytic processes. In addition to singlet oxygen, photoinduced formation of hydroxyl radicals in clay suspensions was reported based on the analysis of final reaction products.[12,13] Spin trapping of OH radicals in the course of a clay-assisted photochemical process was performed in ref. 14. Usually, it is assumed that OH radicals are formed in heterogeneous processes on the surface of clay,[14] but no evidence is provided. It should be noted that both analysis of final reaction products and spin trapping are indirect methods to determine the mechanism of the photochemical reaction. According to our investigation of the photoinduced formation of hydroxyl radicals for an iron-containing montmorillonite clay (KSF) by means of laser flash photolysis,[15] OH radicals occurred in the solution bulk due to photolysis of $[Fe(OH)_{aq}]^{2+}$ complexes formed by iron(III) cations leached from the clay. This result indicated that homogeneous processes were responsible for photocatalysis in this system.

Studying the mechanism of heterogeneous photochemical processes over clay materials by a time-resolved method, such as laser flash photolysis (LFP), is an experimentally attractive challenge. First, the experiments should be performed in suspensions exhibiting significant light scattering which is not favorable for obtaining good LFP signals. Second, it is a problem to discriminate homogeneous and heterogeneous processes.

The aim of this work was to apply LFP to the study of heterogeneous photochemical processes over two types of

[a]*Voevodsky Institute of Chemical Kinetics and Combustion, 3 Institutskaya Str., 630090 Novosibirsk, Russian Federation. E-mail: glebov@kinetics.nsc.ru; Fax: +7 383 3307350; Tel: +7 383 3309150*
[b]*Novosibirsk State University, 2 Pirogova Str., 630090 Novosibirsk, Russian Federation*
[c]*Department of Environmental Science, Hubei Key Lab of Biomass Resource Chemistry and Environmental Biotechnology, School of Resources and Environmental Science, Wuhan University, 430079, P. R. China. E-mail: fengwu@whu.edu.cn*
[d]*Boreskov Institute of Catalysis, 5 Lavrentyev Pr., 630090 Novosibirsk, Russian Federation. E-mail: timofeeva@catalysis.ru*
[e]*Novosibirsk State Technical University, K. Marks Prospect 20, 630092 Novosibirsk, Russian Federation*

This journal is © The Royal Society of Chemistry and Owner Societies 2013

iron-containing systems. The first type of materials were represented by pillared interlayered clays (PILCs) produced from natural iron-containing montmorillonite clays.[16] A way of regulating the textural and physicochemical properties of PILCs is the modification of its structure by exchanging the initial cations for voluminous polynuclear hydroxo cations, *e.g.* Fe^{3+}. Upon heating, the complex cations turn into their respective metal oxides, which act as pillars to fix the silicate layers at a certain distance from one another, thereby producing regular porous structures.[16] Catalysts based on PILCs have been actively investigated in the last decade due to the material's high resistance and stability, the development of microporosity, the large surface area and the presence of acid sites (Brønsted and Lewis sites).[17]

The second type of iron-containing systems was iron-containing mesoporous mesophase iron silicate materials (denoted as Fe-MMM-2[18]). Because of having pore sizes in the range of several nanometers, the internal surface of mesoporous catalysts (MMMs) is opened for a much wider assortment of reagents in comparison with common zeolites.[19] Processes catalyzed by iron-containing MMMs were widely studied in recent years.[18–20]

No leaching of iron cations from both PILCs and MMMs to the solution was detected; therefore, only heterogeneous catalytic processes were possible. In this work, analysis of the data on the laser flash photolysis of phenol in the presence of PILC or MMM was found to give evidence of a significant increase in the quantum yield of the primary intermediates' formation. Data on PILC-induced and MMM-induced photochemistry were compared with that on montmorillonite KSF, for which homogeneous processes were shown to be responsible for the photocatalytic effect.[15]

Phenol was chosen because (i) it is an important industrial product and (ii) its photochemistry has been widely studied (see ref. 21 and references there).

2. Experimental

2.1. Materials

Methyl viologen dichloride hydrate, 98% (Aldrich) was used as a source of MV^{2+} dications. HPLC grade phenol (Aldrich) was used without additional purification. Samples were prepared using deionized water. If necessary, samples were bubbled with argon for 15 min to remove oxygen. Montmorillonite KSF was purchased from Sigma-Aldrich.

2.1.1. Synthesis of PILC materials. The natural aluminosilicate containing more than 95% of a calcium-rich montmorillonite (LAS) and natural aluminosilicate (AS) were obtained from a bed located in Mukhortala (Buryatia) and a bed located in Khumuluut (Mongolia), respectively. The chemical compositions of the clays are shown in Table 1.

The sodium containing layered aluminosilicates (Na-LAS and Na-AS) used for the preparation of the pillared samples were synthesized by the treatment of the natural clays with 1 M NaCl at a ratio of 1 : 100 wt/wt between solid and liquid phases at 80 °C for 2 h.

Table 1 The chemical composition of natural clays

	Chemical composition (wt%)						
Clays	SiO_2	Al_2O_3	SO_2	Fe_2O_3	MgO	CaO	Na_2O
KSF[15]	49.1	16.3	22.3	4.8	4.3	2.3	0.06
AS	60.3	12.3	n.d.	8.3	1.2	1.0	0.15
LAS	65.5	14.3	n.d.	1.1	1.4	1.1	0.3

Synthesis of modified clays Al,Fe-AS and Al,Fe-LAS was performed using a procedure described in ref. 22. Na-clays were stirred (1 wt% solution) in distilled water for about 24 h at 20 °C; then it was dispersed by ultrasonic partition. The Al,Fe-pillaring solutions (Al/Fe = 10/1) were prepared from mixing 0.2 M $AlCl_3$ and 0.1 M $FeCl_3$ with following hydrolysis using NaOH solution (OH/(Al + Fe) = 2.4). A solution of Al/Fe was added to the clay and the mixture was stored for 1 day at room temperature. Then the solid was filtered by suction, washed with distilled water, dried in air and calcinated at 450 °C for 4 h. The chemical composition and structural data of the samples are shown in Table 2.

2.1.2. Synthesis of MMM materials. The synthesis of Fe,Al-MMM-2(2.4) and Fe,Al-MMM-2(4.4) was performed as described in ref. 23. Materials preparation included the mixing of three solutions: (1) 0.2 M aqueous solution of cetyltrimethylammonium bromide (CTAB) (pH 1.0, HCl), (2) 0.12 M aqueous solution of a silica sol (pH 1.0, HCl) and (3) an aqueous Al,Fe-containing solution (Al/Fe 10/1 mol mol ^{1}, OH/(Al + Fe) = 2.4).[24] Then the pH of the synthetic solutions was adjusted to 2.4 or 4.4 by a dropwise addition of an aqueous solution of NaOH (conc.). The molar ratio of Si/CTAB was 5.0. The amount of Al,Fe-containing solution was calculated to achieve an iron content in the resulting catalyst of about 1.1 wt%. After mixing, the synthetic mixture was kept at 323 K for 24 h. The resulting precipitate was filtered with distilled water, dried in air at room temperature for 24 h, and calcinated at 773 K for 8 h. The chemical composition and structural data of Fe,Al-MMM-2 samples are shown in Table 3.

2.2. Instrumental measurements

The concentrations of Fe(II) and Fe(III) in the solutions were determined using typical analytical procedures. Fe(II) was quantified by the addition of 1,10-phenanthroline and

Table 2 Structural properties of clay materials

		Structural data				
Sample	[Fe] (mg g^{-1})	S_{BET} (m^2 g^{-1})	V_{Σ} (cm^3 g^{-1})	V_{μ} (cm^3 g^{-1})	D_{pore} (Å)	d_{001} (Å)
Na-AS	50 ± 1	40	0.058	0.002	118	10
Al,Fe-AS	76 ± 1	47	0.046	0.007	115	11
Na-LAS[22]	8 ± 2	141	0.200	n.d.	57	15
Al,Fe-LAS[22]	17 ± 1	215	0.220	0.051	41	18

[Fe] – the iron content in sample; S_{BET} – specific surface area determined by BET method; V_{Σ} – total pore volume; V_{μ} – micropore volume; D_{pore} – average diameter of pores; d_{001} – interlayer distance.

This journal is © The Royal Society of Chemistry and Owner Societies 2013

Table 3 Structural data of Fe,Al-MMM-2 materials[23]

Sample	Structural data				Chemical composition	
	S_{BET} ($m^2\ g^{-1}$)	S_{ext} ($m^2\ g^{-1}$)	V_{meso} ($cm^3\ g^{-1}$)	d_{10} (nm)	[Fe] ($mg\ g^{-1}$)	Al/Fe ($mol\ mol^{-1}$)
Fe,Al-MMM-2(2.4)	1518	149	0.90	3.9	11 ± 1	6/1
Fe,Al-MMM-2(4.4)	1315	177	0.56	3.8	11 ± 1	12/1

S_{BET} – specific surface area; S_{ext} – external surface area of mesopore aggregates; V_{meso} – mesopore volume; d_{10} – mesopore interlayer spacing; [Fe] – iron content in the material.

measuring the absorption of the Fe(II)-phenanthroline complex at 510 nm.[25] To measure the concentration of Fe(III), it was first reduced to Fe(II) by hydroquinone. When the reduction (monitored by UV spectroscopy) was completed, the concentration of Fe(II) was determined by the 1,10-phenanthroline method.

The porous structure of the materials was determined from the adsorption isotherm of N_2 at 77 K on an Autosorb 6B (Quantachrome) instrument. Software supplied with this instrument was used to calculate the average diameter of pores (D_{pore}). The specific adsorption area (S_{BET}) was calculated by the Brunauer–Emmet–Teller (BET) method. The total pore volume (V_{Σ}) was calculated from the amount of nitrogen adsorbed at a relative pressure 0.99. The specific external surface area (S_{ext}) and the specific micropore volume (V_{μ}) were estimated by the *t*-plot method.[26] The X-ray diffraction patterns were measured on an X-ray diffractometer XRD (ThermoARL) with Cu-K_{α} (λ = 1.5418 Å) radiation.

A laser flash photolysis device based on an LS-2137U Nd:YAG laser (Lotis TII, Belarus) with excitation wavelengths of 266 and 355 nm, pulse duration of 5–6 ns, an illumination spot area of 0.07 cm^2, and an energy per pulse up to 20 mJ was used; the device was similar to the one described in ref. 27. The time resolution of the device was *ca.* 50 ns. Optical spectra were recorded with an Agilent HP 8453 spectrophotometer.

The DR-UV-vis spectra were recorded on a UV-2501 PC Shimadzu spectrophotometer with an IRS-250A accessory in the 190–900 nm range with a resolution of 2 nm. $BaSO_4$ was used as the standard.

2.3. Preparation of suspensions for laser flash photolysis

For the preparation of montmorillonite KSF samples the initial content of clay was 10 g L^{-1}. After the 60 min sedimentation, the upper fraction of the mixture was taken and used for the experiments. The pH value of the solutions was about 3.0, which prevented Fe(III) hydrolysis. If necessary, samples were centrifuged before photolysis (10 min with the rotation speed corresponding to 4400 g).

For the preparation of Na-clay, PILC and MMM aqueous suspensions the initial content of material was 1 g L^{-1}. The suspensions were treated in an ultrasonic bath for 1 h. After settling for 36 hours, the suspended material was precipitated, and the liquid above the precipitate was transparent. When the fraction above the precipitate was sampled and used for the LFP experiments, no signals were obtained. Therefore, the suspensions after ultrasonic bath treatment were settled for 2 h, which resulted in partial precipitation of a suspended material. After that, the fraction above the precipitate was sampled and used in LFP experiments. The typical values of optical density in a 1 cm cell caused by light scattering were 0.8 at 266 nm and 0.6 at 355 nm.

3. Results and discussion

3.1. Investigation of OH radical formation in the course of clay-assisted photolysis

Because the hydroxyl radical does not have a pronounced absorption in the near UV and visible spectral regions, radical generation can be confirmed by a trapping technique, *i.e.* using a radical scavenger. The radical scavenger must satisfy several requirements. Firstly, a scavenger should react with the hydroxyl radical to give a strongly-absorbing intermediate. Secondly, the scavenger should be photochemically inert at the excitation wavelength. Moreover, kinetic parameters of the reaction between the OH radical and a scavenger should be known in the literature.

The formation of $^{\cdot}OH$ in the course of laser flash photolysis (LFP) over clay was investigated in the presence of the radical scavenger methyl viologen (MV^{2+}, Fig. 1a). Methyl viologen has been successfully used for the trapping of hydroxyl radicals.[28,29] The UV absorption spectrum of MV^{2+} is shown in Fig. 1b. Because MV^{2+} absorption at 355 nm is close to zero, it has no photochemistry of its own when excited at this wavelength.

Very different results were obtained in the laser flash photolysis experiments over KSF and PILCs (or MMMs) at 355 nm in the presence of methyl viologen (Fig. 2). In the case of KSF, the formation and decay of intermediate absorption in the region of 400–520 nm was observed (Fig. 2a[15]). This absorption band with the maximum at 470 nm belongs to the adduct of MV^{2+} and a hydroxyl radical ($[MV(^{\cdot}OH)]^{2+}$).[28,29] Very recently, we found[15] that the reaction rate constant of the $[MV(^{\cdot}OH)]^{2+}$ formation in the case of KSF photolysis coincides with the reaction rate constant of the homogeneous reaction between MV^{2+} and $^{\cdot}OH$ ($(2.5 \pm 0.2) \times 10^8\ M^{-1}\ s^{-1}$[29]). Experiments with the centrifuged KSF samples performed in ref. 15 concluded that the formation of OH radicals occurs in the solution due to the direct photolysis of $[Fe(OH)_{aq}]^{2+}$ complexes existing in solutions with pH values of about 3. The

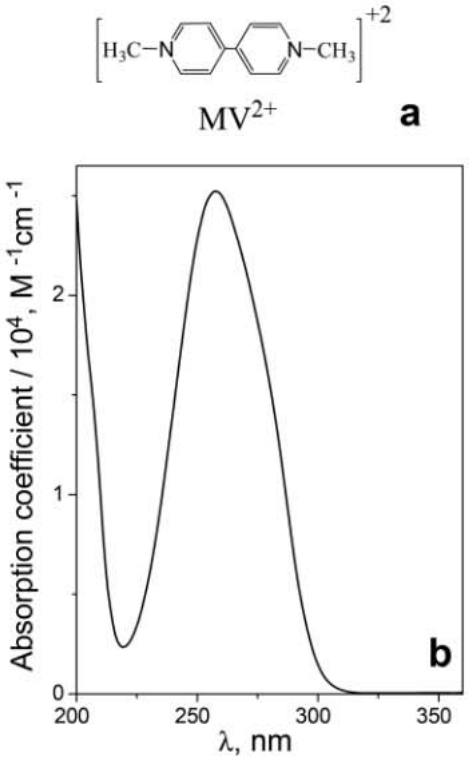

Fig. 1 (a) Structure and (b) UV spectrum of the methyl viologen dication.

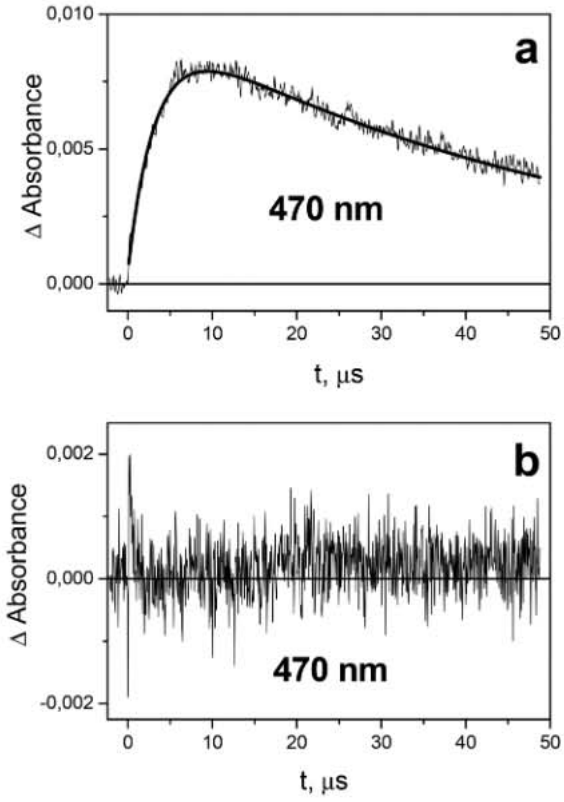

Fig. 2 Laser flash photolysis (355 nm) of clay suspensions (pH 3.0) in the presence of methyl viologen (1×10^{-3} M). 1 cm cell, deaerated samples. Kinetic curves at 470 nm: (a) montmorillonite KSF (10 g L^{-1}, after sedimentation, result is from ref. 15) and (b) Al,Fe-LAS (1 g L^{-1}, after sedimentation, pH 5.5).

Table 4 Concentrations of iron ions leached to the solution bulk from montmorillonite KSF suspensions (10 g L^{-1})

Ions	Fe(III)	Fe(II)
Concentration, M	2.1×10^{-4}	2.8×10^{-4}
% of the maximal possible concentration	3.4	4.6

hydroxocomplexes of Fe(III) are formed by ions leached from the clay material into the solution bulk. Therefore, as concluded in ref. 15, the photocatalytic effect of montmorillonite KSF is caused by homogeneous reactions of Fe(III) species in the solution. The leaching of iron cations from KSF clay to the solution bulk was supported by chemical analysis of the centrifuged clay suspensions (Table 4). 8% of the total amount of iron leaches from KSF. The amount of Fe(II) is even higher than that of Fe(III), but complexes of Fe(II) formed in solution do not demonstrate any remarkable absorption at $\lambda < 250$ nm.[30]

Fig. 2b shows a typical example of a kinetic curve for Al,Fe-LAS photolysis in the presence of MV^{2+}. This is a zero signal. No signals were obtained for all the Na-clays, PILCs and MMMs, both for transparent samples and for turbid suspensions. Therefore, no formation of hydroxyl radicals occurs in the course of PILCs and MMMs photolysis. In addition, no traces of $MV^{\cdot+}$ radical cations, which occurred in the case of the MV^{2+} reaction with the reducing species,[31] were found (like in the case of KSF). Additionally, according to the chemical analysis of solutions after precipitation of PILC and MMM samples, neither Fe(III) nor Fe(II) ions were found. Summarizing the results of the experiments with PILCs and MMMs, one can point out that (i) iron ions do not leach from the particulate PILC and MMM materials to the solution; and (ii) hydroxyl radicals are not formed in the case of 355 nm photolysis in the presence of these materials (neither in homogeneous nor in heterogeneous processes).

Further LFP experiments were performed with excitation at 266 nm. In principle, the possibility exists that OH radicals could be formed upon the heterogeneous process of PILCs and MMMs photolysis at 266 nm. The experiments with MV^{2+} as a scavenger could not be used to rule out this possibility because of the well-known process of direct photolysis of methyl viologen with the formation of $MV^{\cdot+}$ radical cations.[32] Furthermore, we will show that the LFP experiments (266 nm) with phenol as a scavenger of possibly formed OH radicals give kinetic evidence of their absence.

3.2. Laser flash photolysis (266 nm) of phenol in the presence of PILCs and MMMs

The effect of heterogeneous processes induced by PILC and MMM materials on the photolysis of phenol was studied by means of laser flash photolysis (266 nm). Both PILC and MMM samples showed considerable light scattering at the wavelengths of excitation and recording (Fig. 3). When the fraction above the precipitate was sampled and used for the LFP experiments, the results coincided with those obtained for pure phenol solutions. For turbid samples, the registration

This journal is © The Royal Society of Chemistry and Owner Societies 2013

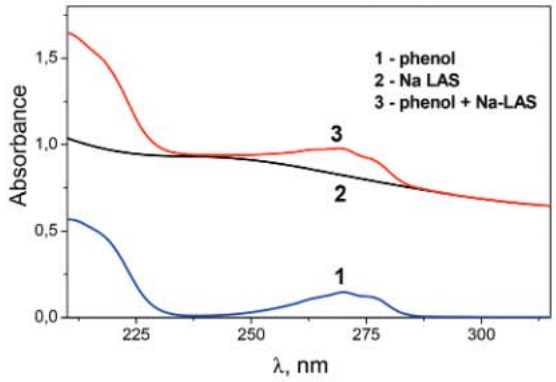

Fig. 3 UV spectra of an aqueous solution of phenol (1.1×10^{-4} M, pH 6.5) – (1), Na-LAS (1 g L^{-1}, pH 6.3) – (2) and a mixture of phenol (1.1×10^{-4} M) and Na-LAS (1 g L^{-1}), pH 6.4 – (3) (1 cm cell).

of intermediate absorption was possible in spite of light scattering.

The results of the experiment on the laser flash photolysis of phenol in the presence of Fe,Al-MMM-2(2.4) are shown in Fig. 4. Fig. 4a demonstrates typical kinetic curves of intermediate absorption changes both in the absence and in the presence

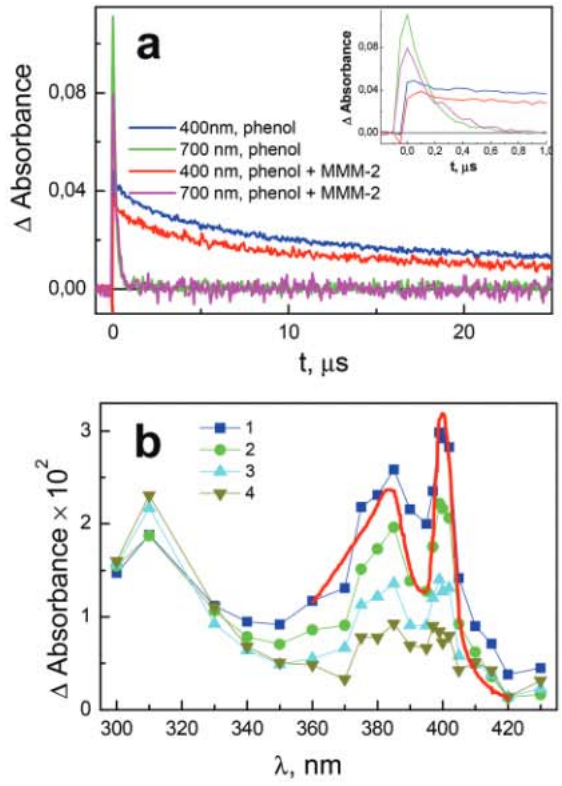

Fig. 4 Laser flash photolysis (266 nm) of an aqueous solution of phenol (2.3×10^{-4} M, pH 6.5) in 1 cm cell, natural content of oxygen, pulse energy 4.2 mJ. (a) Examples of kinetic curves for pure phenol solution and a suspension of Fe,Al-MMM-2(2.4) (1 g L^{-1}). Inset shows the initial part of the kinetic curves. Black lines correspond to zero signals. (b) Temporal evolution of the intermediate absorption spectrum of phenol in the presence of Fe,Al-MMM-2(2.4). Curves 1–4 correspond to time intervals 0.8; 4; 14; 48 μs after the laser pulse, respectively. Red line – spectrum of phenoxyl radical taken from ref. 37.

of catalyst. Kinetic curves obtained by phenol photolysis in the presence of Fe,Al-MMM-2(2.4) at two characteristic wavelengths (400 and 700 nm) are shown in Fig. 4a. The inset in Fig. 4a shows the initial parts of the kinetic curves. As evident from the results presented in Fig. 4a, the characteristic times of the intermediate absorption decay at 700 and 400 nm are very different. Absorption in the region of 700 nm decays with the characteristic time of *ca.* 200 ns (see the inset in Fig. 4a), while absorption at 400 nm decays more slowly. Therefore, at least two different intermediates are formed under the action of the laser pulse. These intermediates are hydrated electrons and phenoxyl radicals. The spectral signature of the hydrated electron is the wide absorption band with its maximum in the region of 720 nm,[33,34] with the maximal extinction coefficient equal to 22 700 M^{-1} cm^{-1}.[33] e_{aq}^- reacts with oxygen with the rate constant 1.9×10^{10} M^{-1} s^{-1}.[33]

Fig. 4b shows the evolution of the intermediate absorption spectra for (phenol + MMM) system. The kinetic curves and intermediate absorption spectra are similar for all Na-clays, PILCs and MMM materials. The characteristic spectrum of intermediate absorption containing two peaks at 380 and 400 nm (Fig. 4b) belongs to the phenoxyl radical PhO˙. It could be obtained by direct photolysis of aqueous phenol solutions in the UV region,[35] by photolysis of the $[Fe(OH)_{aq}]^{2+}$ complex in the presence of phenol[36] or by pulse radiolysis.[37] The red line in Fig. 4b is the PhO˙ spectrum taken from ref. 37. For the extinction coefficient of PhO˙ at 400 nm the values of 2200 M^{-1} cm^{-1} [37,38] and 2625 M^{-1} cm^{-1} [39] are available in the literature.

It was important to ensure that the route of PhO˙ formation by the reaction of phenol with OH radicals did not exist. One could assume that photolysis of PILCs and MMMs at 266 nm results in the formation of OH radicals, which could react with phenol. Let us consider this possibility.

The reaction between ˙OH and phenol was studied by means of pulse radiolysis[38,40] and laser flash photolysis.[36] The addition of a hydroxyl radical to the phenol ring results in the formation of isomeric dihydroxycyclohexadienyl radicals with the common formula $Ph(OH)_2$˙. The UV spectra of these radicals are similar; they show a maximum at 335 nm. $Ph(OH)_2$˙ radicals are transformed to PhO˙ having characteristic absorption peaks at 380 and 400 nm. The reaction mechanism is represented by reactions 1–6, and the rate constants are collected in Table 5. The $Ph(OH)_2$˙ → PhO˙ reaction is catalyzed by both H^+ and OH^- ions.[38]

$$OH^{\cdot} + C_6H_5OH \rightarrow (o\text{-})p\text{-}C_6H_5(OH)^{\cdot}{}_2 \qquad (1, 2)$$

Table 5 Rate constants of reactions important for PhO radicals formation[36a]

Reaction	$k \times 10^{-9}$ (M^{-1} s^{-1})
1	8
2	6
3	1
4	0.1
5, 6	2.9

$$(o\text{-})p\text{-}C_6H_5(OH)^{\cdot}{}_2 + H^+ \rightarrow C_6H_5O^{\cdot} + H_2O + H^+ \qquad (3,4)$$

$$(o\text{-})p\text{-}C_6H_5(OH)^{\cdot}{}_2 + C_6H_5O^{\cdot} \rightarrow (o\text{-})p\text{-}C_6H_4(OH)_2 + C_6H_5OH \qquad (5,6)$$

The characteristic time of PhO$^{\cdot}$ formation in 3 mM phenol solution at pH 3.5 was *ca.* 20 μs.[38] For our typical experimental conditions (0.1 mM of phenol, pH 5–6) the characteristic time of PhO$^{\cdot}$ formation could be estimated as *ca.* 10 ms. It means that PhO radicals could not be formed at all, because the alternative ways of Ph(OH)$_2^{\cdot}$ decay (*e.g.* self-reaction) resulting in other products are also possible.

However, the characteristic time of PhO$^{\cdot}$ formation in our experiments was less than, or at least comparable with, the time resolution of the laser flash photolysis setup (50 ns, Fig. 4 and 5). The addition of Na-clays, PILCs and MMMs did not affect the shape of the experimental kinetic curves (Fig. 5a and b). It means that the reaction pathway starting with the OH radical formation upon 266 nm irradiation of Na-clays, PILCs and MMMs could be ruled out.

The mechanism of phenol photolysis in aqueous solutions is rather complicated.[41] It includes photoionization, photodissociation and triplet state formation. Photoionization results in the formation of a primary pair hydrated electron–radical cation PhOH$^{\cdot+}$ (eqn (7)[42,43]). PhOH$^{\cdot+}$ rapidly dissociates with the formation of a long-living phenoxyl radical (eqn (8)[43]). Geminate recombination of the ejected electron and the proton on a very fast time scale (eqn (9)) may be responsible for a smaller yield of solvated electrons in comparison with that of PhO radicals.[44] Direct photodissociation of phenol (eqn (10)) in aqueous solutions is improbable.[45] In addition to one-photon processes, biphotonic photoionization *via* the triplet state of phenol (eqn (11) and (12)) is possible.[46]

$$PhOH \xrightarrow[H_2O]{h\nu} PhOH^{\cdot+} + e^-_{aq} \qquad (7)$$

$$PhOH^{\cdot+} \rightarrow PhO^{\cdot} + H^+ \qquad (8)$$

$$\{H^+ + e^-_{aq}\}_{cage} \rightarrow H^{\cdot} \qquad (9)$$

$$PhOH \xrightarrow[H_2O]{h\nu} PhO^{\cdot} + H^{\cdot} \qquad (10)$$

$$PhOH \xrightarrow[H_2O]{h\nu} (PhOH)^{*T} \qquad (11)$$

$$(PhOH)^{*T} \xrightarrow[H_2O]{h\nu} PhOH^{\cdot+} + e^-_{aq} \qquad (12)$$

Kinetic curves of PhO radical decay in pure phenol solutions (1.1×10^{-4} M) were recorded at different energies of an exciting laser pulse (Fig. 5a). The initial absorption of PhO radicals (Fig. 5c, curve 1) linearly depends on the exciting light intensity indicating low probability of two-photon processes.

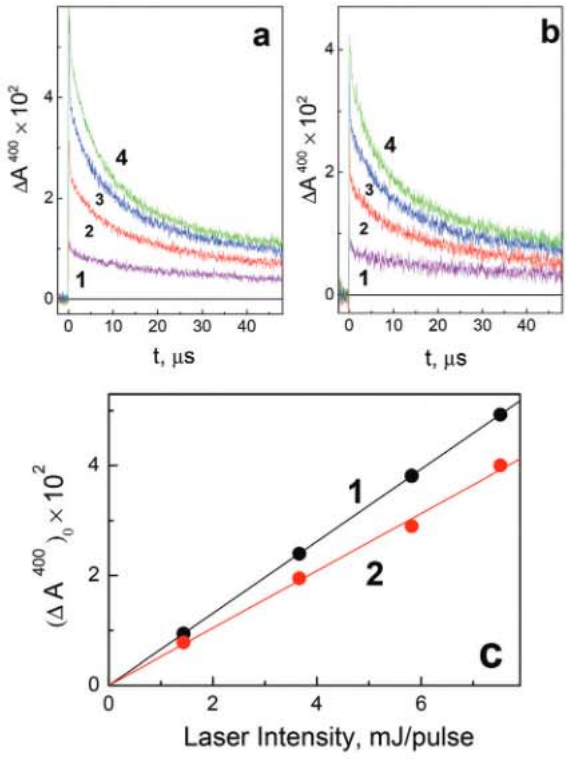

Fig. 5 Laser flash photolysis (266 nm) of phenol (1.1×10^{-4} M, pH 6.5) in aqueous solutions. (a) Kinetic curves at 400 nm in the absence of clay material; (b) kinetic curves at 400 nm in the presence of Na-LAS (1 g L^{-1}). Correction to the clay signal was performed. Curves 1–4 in panels (a) and (b) correspond to different energies of exciting laser pulse. (c) Peak values of initial PhO radical absorption (400 nm) as functions of the laser pulse energy. Curves 1 and 2 correspond to sets of kinetic curves (a) and (b).

3.3. Primary quantum yields of PhO$^{\cdot}$ formation caused by phenol photolysis in the presence of clay materials

Information concerning the effect of clay materials on the PhO radical yield was extracted from the dependencies of the initial radical absorption on the energy of the laser pulses. Fig. 5 shows typical kinetic curves of phenoxyl radical decay for pure phenol (Fig. 5a) and for phenol in the presence of Na-LAS (Fig. 5b). Dependencies of the initial PhO$^{\cdot}$ absorption on exciting pulse energy (Fig. 5c) allow one to calculate the primary quantum yields of radical formation.

The experiments with clay materials were performed in turbid solutions with significant light scattering by the clay material particles (Fig. 3). If clay material does not affect the photolysis of phenol, the initial concentration of radicals should be proportional to the intensity of light absorbed by phenol, which is calculated using eqn (13):

$$I_{Abs}^{Phenol} = I_0 \times \left(1 - 10^{-(D_{Phenol}+D_{Clay})}\right) \times \frac{D_{Phenol}}{D_{Phenol}+D_{Clay}} \qquad (13)$$

where I_0 is the total intensity of incident light and all the optical densities (D) rely on the excitation wavelength (266 nm). The obtained results indicate conclusively that the yields of radicals have not dropped proportional to the intensity of light absorbed by phenol. As can be seen from Table 6, a significant increase in the quantum yield of PhO$^{\cdot}$ formation is observed for Na-LAS and Al,Fe-LAS and MMM materials in comparison with Na-AS and Al,Fe-AS. The quantum yield of

This journal is © The Royal Society of Chemistry and Owner Societies 2013

Table 6 Relative quantum yields of PhO radical formation upon the photolysis of phenol in the presence of Na-clays and Fe-containing samples

Sample	[Fe][a] (mg g^{-1})	pH (1 g L^{-1})	φ/φ_0[b]
Na-AS	50 ± 1	8.0	1.2 ± 0.2
Al,Fe-AS	76 ± 1	6.1	1.2 ± 0.2
Na-LAS	8 ± 2	6.3	1.9 ± 0.3
Al,Fe-LAS	17 ± 1	5.5	1.5 ± 0.2
Fe,Al-MMM-2(2.4)	11 ± 1	4.5	1.8 ± 0.2
Fe,Al-MMM-2(4.4)	11 ± 1	5.3	1.6 ± 0.2

[a][Fe] – iron content in the material. [b]φ/φ_0 – the ratio of primary quantum yields of phenol photolysis (266 nm) in the presence and in the absence of catalysts.

PhO˙ formation decreases in the order: Na-LAS > Al,Fe-MMM-2(2.4) > Al,Fe-MMM-2(4.4) > Al,Fe-LAS > Na-AS ~ Al,Fe-AS.

It is interesting that no correlation between iron content in the materials and quantum yield of radical formation was obtained. In spite of Na-AS and Al,Fe-AS materials having a 5 to 10 times higher content of Fe(III) than that of other materials, they demonstrate the weakest effect on photolysis.

Several explanations for this fact could be offered. First, one can assume that the rate of radical formation is affected by the state of the iron species in the matrix. DR-UV-Vis spectra of the Fe-containing materials are shown in Fig. 6. As can be seen from the experimental evidence, the band in the region of 240–280 nm is observed in the spectra of the samples. This band is usually assigned to the low-energy charge transfer between the oxygen ligands and Fe^{3+} ions, *i.e.* the $t_1 \rightarrow t_2$ and $t_1 \rightarrow e$ transitions for Fe^{3+} in the $[FeO_4]$ tetrahedral group.[47] The position of this band maximum depends on the amount of iron in the samples. Thus, a low amount of iron in Al,Fe-LAS (17 mg g^{-1}) leads to the appearance of this band at 256 nm, while a high amount of iron in Al,Fe-AS (76 mg g^{-1}) leads to the red shift of this band to 285 nm. As can be seen from Table 6, these shifts are in agreement with the quantum yield of radicals. This phenomenon indicates that the electron density on the iron cation affects the rate of radical formation in the course of photolysis. A similar effect can be revealed by comparison of Al,Fe-MMM-2(2.4) and Al,Fe-MMM-2(4.4). A weak red shift from 267 nm (Al,Fe-MMM-2(2.4)) to 273 nm (Al,Fe-MMM-2(4.4)) is observed after increasing the Al content. These shifts in spectra are likely arising from the different coordination of iron species. Additionally, the oligomeric state of iron species in the PILCs should be taken into account. According to DR-UV-vis spectra of the samples (Fig. 6), the intensity of bands in the region of 300–600 nm increases with increasing iron content in PILCs.

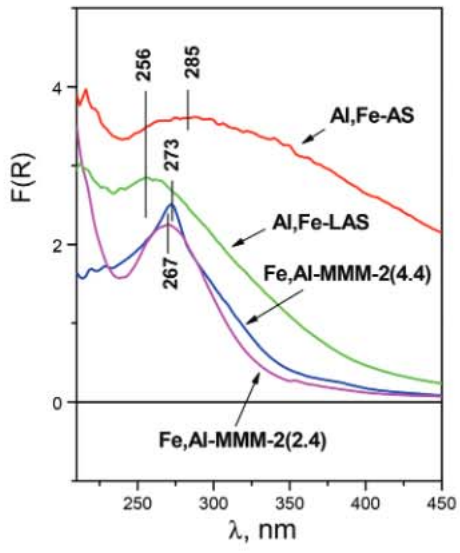

Fig. 6 DR-UV-Vis spectra of Al,Fe-containing materials.

Surface acidity of samples could be another reason for this phenomenon. In our previous work[18,23] it was demonstrated that insertion of Al species into the framework of the silicate MMM matrix increased the surface acidity, which was accompanied by a decrease in the PhOH adsorption capacity. These data show us that high surface acidity favors a decrease in amount of PhO˙ formed.

To ensure that the addition of scattering media to the solutions of phenol should result in a decrease of the photolysis quantum yield proportional to the intensity of light absorbed by phenol (eqn (13)), control experiments were performed. MgO powder was added to aqueous phenol solution to obtain a scattering medium which does not affect the photolysis. Because MgO in aqueous solutions gives an alkali reaction, the control experiments were performed in alkaline media (pH 11.8). At these conditions, phenol forms the phenolate anion, PhO . According to ref. 48, the quantum yields of both e_{aq} and PhO˙ formation upon PhO photolysis at 254 nm in aqueous solutions (eqn (14)) is 0.17.

$$PhO^- \xrightarrow{h\nu} PhO^{\cdot} + e^-_{aq} \qquad (14)$$

The results of the control experiments are shown in Fig. 7. Fig. 7a demonstrates the UV spectra of alkaline phenol solutions with added MgO powder. Dashed lines correspond to spectra provided by light scattering by MgO suspension, and full lines are spectra provided by scattering of MgO and absorption of phenolate-ion. Fig. 7b shows the dependence of quantum yield of PhO radicals formation on optical density provided by phenol scattering. In calculation of quantum yield, correction to the light absorbed by phenol was made using eqn (13) (D_{MgO} was taken instead of D_{Clay}). Independence of the quantum yield of PhO˙ formation on the content of scattering MgO particles demonstrates the validity of the approach used for the calculation of quantum yield for the systems (phenol + catalyst).

3.4. Possible reasons for the quantum yield increase in the presence of Fe-containing materials

In the experiments with Na-clays, PILCs and MMMs the possibility of PhO˙ formation due to the reaction between phenol and OH radicals resulting from the 266 nm photolysis of the catalyst was ruled out (see Section 3.2).

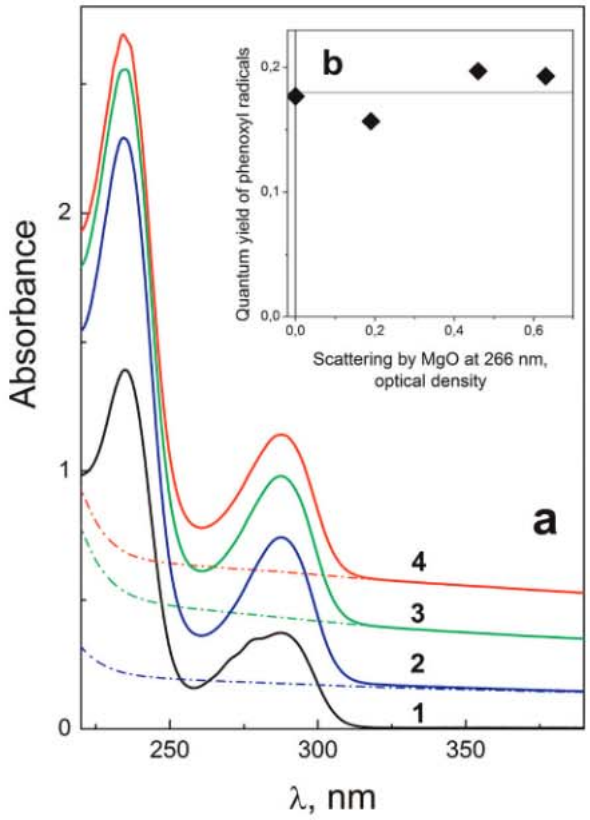

Fig. 7 (a) UV spectra of system in experiments on laser flash photolysis (266 nm) of phenol in the presence of scattering particles of MgO (dashed lines – spectra provided by light scattering by MgO suspension, solid lines – spectra provided by light scattering of MgO and absorption of phenol). Curves 1–4 correspond to 0; 2; 4; 8 mg ml^{-1} of MgO, respectively. (b) Correlation between the quantum yield of PhO radical formation and MgO content in the samples (see text). Experimental conditions: mixture of 2.4×10^{-4} M phenol (pH 11.9) and MgO powder in a 1 cm cell.

Two possibilities for the increase in the quantum yield of $PhO^{\cdot}$ formation caused by PILC and MMM can be considered.

1. An electron transfer from a phenol molecule situated in the solution bulk to a Fe(III) cation located on the surface of a clay (or MMM catalyst) particle is possible (eqn (15))

$$PhOH + Fe^{III}_{surface} \xrightarrow{h\nu} PhOH^{\cdot +} + Fe^{II}_{surface} \quad (15)$$

Reaction (15) is followed by a proton transfer from the $PhOH^{\cdot +}$ radical cation to the solvent *via* reaction 8.

2. Another possibility is that a phenol molecule is adsorbed to the surface of an iron-containing particle in the catalyst suspension. In this case, a reaction similar to (15) occurs on the surface of catalyst.

$$\{PhOH + Fe^{III}\}_{surface} \xrightarrow{h\nu} \{PhOH^{\cdot +} + Fe^{II}\}_{surface} \quad (16)$$

After formation of the radical cation $PhOH^{\cdot +}$ on the surface, it transfers a proton to the solvent with the formation of $PhO^{\cdot}$. The phenoxyl radical could be located either in the solution bulk or on the surface of catalyst. Re-oxidation of the surface Fe(II) cations by dissolved oxygen could lead to the restoration of the catalyst.

Conclusions

This work gives examples of both homogeneous and heterogeneous photochemical processes with the participation of iron-containing clays, layered materials and mesoporous silica (MMM) materials. In the case of montmorillonite KSF, Fe(III) anions were found to leach into the solution, and the photocatalytic effect was explained by a homogeneous process of $[Fe(OH)_{aq}]^{2+}$ complex photolysis with OH radical formation. At the same time, leaching of Fe(III) into the solution was negligible in the presence of PILC and MMM materials. The effect of these materials on the photoionization of phenol was explained by the heterogeneous processes. In general, when assessing the effect of clays and other layered materials on the photodegradation of organic contaminants in natural aqueous systems, one should take into account both homogeneous and heterogeneous pathways of photolysis.

Acknowledgements

This work was supported by the Russian Foundation of Basic Research (grants no. 11-03-268-a, 12-03-00482-a, 12-03-91153-GFEN-a) and the National Science Foundation of China (NSFC-RFBR project no. 21211120159).

Notes and references

1 Y. Soma and M. Soma, *Environ. Health Perspect.*, 1989, **83**, 205.
2 K. Beneke and G. Lagaly, *ECGA Newsl.*, 2002, **5**, 57.
3 J. Feng, X. Hu and P. L. Yue, *Environ. Sci. Technol.*, 2004, **38**, 5773.
4 J. H. Ramirez, C. A. Costa, L. M. Madeira, G. Malta, M. A. Vicente, M. L. Rojas-Cervantes, A. J. Lopez-Peinado and R. M. Martin-Aranda, *Appl. Catal., B*, 2007, **71**, 44.
5 (*a*) T. Katagi, *J. Agric. Food Chem.*, 1990, **38**, 1595; (*b*) T. Katagi, *J. Agric. Food Chem.*, 1991, **39**, 1351; (*c*) T. Katagi, *Rev. Environ. Contam. Toxicol.*, 2004, **182**, 1.
6 T. Tietjen, A. V. Vahatalo and R. G. Wetzel, *Aquat. Sci.*, 2005, **67**, 51.
7 (*a*) L. Kong and J. L. Ferry, *Environ. Sci. Technol.*, 2003, **37**, 4894; (*b*) L. Kong and J. L. Ferry, *J. Photochem. Photobiol., A*, 2004, **162**, 415.
8 (*a*) J. Li, F. Wu, N. Deng, E. M. Glebov and N. M. Bazhin, *React. Kinet. Catal. Lett.*, 2008, **95**, 247; (*b*) Y. Liu, K. Wan, N. Deng and F. Wu, *React. Kinet. Mech. Catal.*, 2010, **99**, 493; (*c*) J. Li, F. Wu, G. Mailhot and N. Deng, *J. Hazard. Mater.*, 2010, **174**, 368; (*d*) Y. Liu, X. Zhang and F. Wu, *Appl. Clay Sci.*, 2010, **49**, 182; (*e*) J. Li, G. Mailhot, F. Wu and N. Deng, *Photochem. Photobiol. Sci.*, 2012, **11**, 1880.
9 Z. Xiong, Y. Xu, L. Zhu and J. Zhao, *Langmuir*, 2005, **21**, 10602.
10 J. Menesi, L. Korosi, E. Bazso, V. Zollmer, A. Richard and I. Dekany, *Chemosphere*, 2008, **70**, 538.

This journal is © The Royal Society of Chemistry and Owner Societies 2013

11 Z. Xiong, Y. Xu, L. Zhu and J. Zhao, *Environ. Sci. Technol.*, 2005, **39**, 651.
12 T. Katagi, *J. Agric. Food Chem.*, 1993, **41**, 2178.
13 F. Wu, J. Li, Zh. Peng and N. Deng, *Chemosphere*, 2008, **72**, 407.
14 D. Gournis, M. A. Karakassides and D. Petridis, *Phys. Chem. Miner.*, 2002, **29**, 155.
15 X. Zhang, F. Wu, N. Deng, I. P. Pozdnyakov, E. M. Glebov, V. P. Grivin, V. F. Plyusnin and N. M. Bazhin, *React. Kinet. Catal. Lett.*, 2008, **94**, 207.
16 M. N. Timofeeva and S. Ts. Khankhasaeva, *Kinet. Catal.*, 2009, **50**, 63.
17 (*a*) N. Crowther and F. Larachi, *Appl. Catal., B*, 2003, **46**, 293; (*b*) J. Carriazo, E. Guelou, J. Barrault, J. M. Tatibouet, R. Molina and S. Moreno, *Catal. Today*, 2005, **107/108**, 126; (*c*) M. N. Timofeeva, S. Ts. Khankhasaeva, S. V. Badmaeva, A. I. Chuvilin, E. B. Burgina, A. B. Ayupov, V. N. Panchenko and A. V. Kulikova, *Appl. Catal., B*, 2005, **59**, 243; (*d*) J. T. Kloprogge, L. V. Duong and R. L. Frost, *Environ. Geol.*, 2005, **47**, 967; (*e*) A. Gil, S. A. Korili and M. A. Vicente, *Catal. Rev. Sci. Eng.*, 2008, **50**, 153; (*f*) M. N. Timofeeva, V. N. Panchenko, A. Gil, V. P. Doronin, A. V. Golovin, A. S. Andreev and V. A. Likholobov, *Appl. Catal., B*, 2011, **104**, 54.
18 M. N. Timofeeva, M. S. Mel'gunov, O. A. Kholdeeva, M. E. Malyshev, A. N. Shmakov and V. B. Fenelonov, *Appl. Catal., B*, 2007, **75**, 290.
19 A. Corna, *Chem. Rev.*, 1997, **97**, 2373.
20 (*a*) P. Ratnasamy and R. Kumar, *Catal. Today*, 1991, **9**, 329; (*b*) Y. Wang, Q. Zhang, T. Shishido and K. Takehira, *J. Catal.*, 2002, **209**, 186; (*c*) T. Kawabata, Y. Ohishi, S. Itsiki, N. Fujisaki, T. Shihido, K. Takaki, Q. Zhang, Y. Wang and K. Takehira, *J. Mol. Catal. A: Chem.*, 2005, **236**, 99; (*d*) F. Martinez, G. Calleja, J. A. Melero and R. Molina, *Appl. Catal., B*, 2006, **66**, 198; (*e*) R. Molina, F. Martinez, J. A. Melero, D. H. Bremner and A. G. Chakinala, *Appl. Catal., B*, 2006, **60**, 181.
21 S. Rayne, K. Forest and K. J. Friesen, *Environ. Int.*, 2009, **35**, 425.
22 M. N. Timofeeva, S. Ts. Khankhasaeva, Yu. A. Chesalov, S. V. Tsybulya, V. N. Panchenko and E. Ts. Dashinamzhinova, *Appl. Catal., B*, 2009, **88**, 127.
23 M. N. Timofeeva, M. E. Malyshev, V. N. Panchenko, A. N. Shmakov, A. G. Potapov and M. S. Mel'gunov, *Appl. Catal., B*, 2010, **95**, 110.
24 A. Oszko, J. Kiss and I. Kiricsi, *Phys. Chem. Chem. Phys.*, 1999, **1**, 2565.
25 K. C. Kurien, *J. Chem. Soc. B*, 1971, 2081.
26 S. J. Gregg and K. S. W. Sing, *Adsorption Surface Area and Porosity*, Academic Press, 1991.
27 I. P. Pozdnyakov, V. F. Plyusnin, V. P. Grivin, D. Yu. Vorobyev, N. M. Bazhin, S. Pages and E. Vauthey, *J. Photochem. Photobiol., A*, 2006, **181**, 37.
28 L. K. Patterson, R. D. Small and J. C. Scaiano, *Radiat. Res.*, 1977, **72**, 218.
29 S. Solar, W. Solar, N. Getoff, J. Holcman and K. Sehested, *J. Chem. Soc., Faraday Trans. 1*, 1985, **81**, 1101.
30 J. Jortner and G. Stein, *J. Phys. Chem.*, 1962, **66**, 1264.
31 (*a*) D. R. Prasad, M. Z. Hoffman, Q. G. Mulazzani and M. A. J. Rodgers, *J. Am. Chem. Soc.*, 1986, **108**, 5135; (*b*) E. M. Glebov, I. P. Pozdnyakov, V. P. Grivin, V. F. Plyusnin, X. Zhang, F. Wu and N. Deng, *Photochem. Photobiol. Sci.*, 2011, **10**, 425.
32 (*a*) J. F. McKellar and P. H. Turner, *Photochem. Photobiol.*, 1971, **13**, 437; (*b*) F. Wu, N. Deng, E. M. Glebov, I. P. Pozdnyakov, V. P. Grivin, V. F. Plyusnin and N. M. Bazhin, *Russ. Chem. Bull.*, 2007, **56**, 900.
33 G. V. Buxton, C. L. Greenstock, W. P. Helman and A. B. Ross, *J. Phys. Chem. Ref. Data*, 1988, **17**, 513.
34 P. M. Hare, E. A. Price and D. M. Bartels, *J. Phys. Chem. A*, 2008, **112**, 6800.
35 E. J. Land, G. Porter and E. Strachan, *Trans. Faraday Soc.*, 1961, **57**, 1885.
36 (*a*) I. P. Pozdnyakov, Yu. A. Sosedova, V. F. Plyusnin, V. P. Grivin, D. Yu. Vorob'ev and N. M. Bazhin, *Russ. Chem. Bull.*, 2004, **53**, 2715; (*b*) I. P. Pozdnyakov, Yu. A. Sosedova, V. F. Plyusnin, E. M. Glebov, V. P. Grivin, D. Yu. Vorobyev and N. M. Bazhin, *Int. J. Photoenergy*, 2004, **6**, 89.
37 R. J. Field, N. V. Raghavan and J. G. Drummer, *J. Phys. Chem.*, 1982, **86**, 2443.
38 E. J. Land and M. Ebert, *Trans. Faraday Soc.*, 1967, **63**, 1181.
39 R. Hermann, G. R. Mahalaxmi, T. Jochum, S. Naumov and O. Brede, *J. Phys. Chem. A*, 2002, **106**, 2379.
40 N. V. Raghavan and S. Steenken, *J. Am. Chem. Soc.*, 1980, **102**, 3495.
41 C. Richard and G. Grabner, Mechanism of phototransformation of phenol and derivatives in aqueous solution, in *The Handbook on Environmental Chemistry, vol. 2, Part L Environmental Photochemistry*, ed. P. Boule, Springer-Verlag, Berlin, Heidelberg, 1999, pp. 217–240.
42 D. Creed, *Photochem. Photobiol.*, 1984, **39**, 563.
43 O. Brede, T. Leichtner, S. Kapoor, S. Naumov and R. Hermann, *Chem. Phys. Lett.*, 2002, **366**, 377.
44 Y. Kajii and R. W. Fessenden, *Res. Chem. Intermed.*, 1999, **25**, 567.
45 J. Zechner, G. Kohler, G. Grabner and N. Getoff, *Chem. Phys. Lett.*, 1976, **37**, 297.
46 (*a*) J. Feitelson, E. Hayon and J. Treinin, *J. Am. Chem. Soc.*, 1973, **95**, 1025; (*b*) D. V. Bent and E. Hayon, *J. Am. Chem. Soc.*, 1975, **97**, 2599.
47 B. N. Figgis, *Introduction to Ligand Fields*, Wiley-Interscience, New York, 1966, p. 351.
48 G. Grabner, G. Kohler, J. Zechner and N. Getoff, *Photochem. Photobiol.*, 1977, **26**, 449.